Numerical investigation on implementing Oxy-Fuel Combustion (OFC) in an ethanol-gasoline Dual-Fuel Spark Ignition (DFSI) engine

Xiang Li [a], Yiqiang Pei [b], Tahmina Ajmal [a], Khaqan-Jim Rana [a], Abdel Aitouche [c, d], Raouf Mobasheri [c, d], Zhijun Peng [e,*],

[a] School of Computer Science and Technology, University of Bedfordshire, Luton, UK

[b] State Key Laboratory of Engines, Tianjin University, Tianjin, China

[c] Univ. Lille, CNRS, Centrale Lille, UMR 9189 - CRIStAL - Centre de Recherche en Informatique Signal et Automatique de Lille, F-59000 Lille, France

[d] Junia, Smart Systems and Energies, F-59000 Lille, France

[e] School of Engineering, University of Lincoln, Lincoln, UK

* Corresponding author at: School of Engineering, University of Lincoln, Lincoln LN6 7TS, UK.

E-mail address: jpeng@lincoln.ac.uk (Z. Peng).

Abstract

To decrease even eliminate Carbon Dioxide (CO_2) emissions for mitigating global warming, various technologies are being developed on combustion engines. In the research presented in this paper, a numerical investigation of Oxy-Fuel Combustion (OFC) technology on an ethanol-gasoline Dual-Fuel Spark Ignition (DFSI) engine under economical oxygen consumption at low and mid-high loads was performed by one-dimensional computer simulation. It is demonstrated that under OFC mode without other optimisation, Brake Mean Effective Pressure (BMEP) can meet the requirement at mid-high load, but it has a considerable decline at low load compared to Conventional Air Combustion (CAC) mode. Moreover, there is a considerable deterioration in Brake Specific Fuel Consumption

(BSFC) compared to that of CAC mode. A practical method is proposed to optimise the DFSI engine performance under OFC mode by changing intake charge components and utilising appropriate Water Injection (WI) strategies. BMEP increases approximately 0.05 bar at low load. BSFC has a reduction of 3.35% and 1.82% at low load and mid-high load, respectively.

Keywords

Oxy-Fuel Combustion (OFC); Dual-Fuel Spark Ignition (DFSI) engine; Ethanol; Gasoline; Computer simulation

1. Introduction

The global warming has been a severe problem in recent decades, primarily related to the increase of Greenhouse Gas (GHG) emissions. In order to ease the deterioration of climate crisis, carbon neutrality has been proposed as a promising approach [1][2]. Some advanced powertrain technologies have been utilised, such as battery electric, hybrid electric, plug-in hybrid electric and fuel-cell electric [3][4][5]. These technologies have been demonstrated to reduce Carbon Dioxide (CO_2) emissions, whereas they are mostly applied in passenger cars rather than boats due to the high cost and low torque output.

Oxy-Fuel Combustion (OFC) was proposed as a practical and revolutionary technology of Carbon Capture and Storage (CCS) to eliminate CO_2 emission for non-road machinery powered by fossil fuel [6]. The general configuration of OFC technology in Internal Combustion (IC) engines can be summarised as Fig. 1, and the chemical reaction is illustrated in Equation (1). By replacing air with oxygen for fuel combustion, the products merely contain CO_2 and H_2O. Then, a part of exhaust gas is recirculated to back to cylinder, and extra CO_2 in the exhaust can be separated, captured and stored.

The comparison of physicochemical properties between CO_2 and nitrogen is given in Table 1, which have significant impacts on OFC and Conventional Air Combustion (CAC) [7][8]. The molecular weight of CO_2 is 1.57 times that of nitrogen. Thus, the heat capacity on mole basis is much higher than that of nitrogen, leading to a negative impact on the combustion temperature under OFC. The thermal conductivity of CO_2 is a bit higher than nitrogen, so there is little difference in conductive heat transfer under OFC compared to CAC. Besides, compared to CAC, the lower thermal diffusivity and oxygen diffusion of CO_2 would reduce the rates of chemical reaction and heat release in the early stage of consumption under OFC.

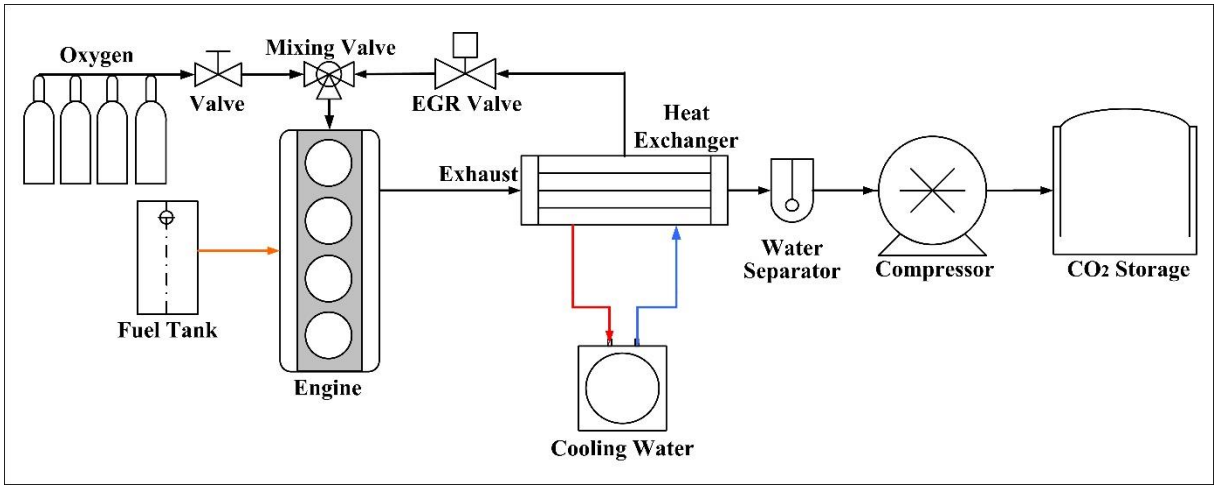

Fig. 1. A general flow chart of a kind oxy-fuel combustion technology for IC engine

$$C_xH_yO_z + \left(x + \frac{y}{4} - \frac{z}{2}\right) O_2 \rightarrow xCO_2 + \frac{y}{2} H_2O \quad (1)$$

Table 1. Physicochemical properties of CO_2 and nitrogen (N_2) at 1000 k and 0.1 MPa [7][8]

Property	CO_2	N_2	Ratio (CO_2/ N_2)
Molecular weight	44	28	1.57
Density (kg/m^3)	0.5362	0.3413	1.57
Kinematic viscosity (m^2/s)	7.69e-5	1.2e-4	0.631
Specific heat capacity (kJ/kg K)	1.2343	1.1674	1.06

Thermal conductivity (W/m K)	7.057e-2	6.599e-2	1.07
Thermal diffusivity (m^2/s)	1.1e-4	1.7e-4	0.644
Mass diffusivity of O_2 (m^2/s)	9.8e-5	1.3e-4	0.778
Prandtl number	0.7455	0.7022	1.06
Emissivity and absorptivity	>0	~0	-

Regarding research on OFC of Compression Ignition (CI) engines, an idea named Closed Cycle Diesel Engine (CCDE) was proposed in the early 1980s [9][10]. In recent years, Wu et al. [11][12][13] conducted a series of investigations for improving the combustion and emission performance of CCDE with various intake gas contents. Mobasheri et al. [14] performed a numerical study for the effects of different diluent strategies on Homogenous Charge Compression Ignition (HCCI) engine under OFC mode. Li et al. [15] numerically investigated the implementation of OFC on a practical diesel engine at the economical oxygen-fuel ratios.

Regarding Spark Ignition (SI) engines, Bilger [16] proposed a novel system called Internal Combustion Rankine Cycle (ICRC) engine, which feature is that preheated water is directly injected into cylinders for controlling combustion process. Wu et al. [17-22] applied the idea of ICRC to practical Port Fuel Injection (PFI) SI engine fuelled with propane. In these studies, the oxygen fraction ranges from 40% to 55% in volume. It was founded that the power performance, thermal efficiency and emissions behaviour of ICRC engine can be optimised with various strategies.

According to the previous research outcomes, it is of great value to implement OFC technology on IC engines. However, the existing publications of OFC technology in SI engines are mostly conducted on PFI engines with an alternative fuel (propane) under the intake of high oxygen fractions [17-22]. Less consideration has been paid to implementing OFC in engines with Gasoline Direct Injection (GDI) technology. Besides, as there is an ever-increasing concern for reducing IC engines' particulate emissions, alcohols have been promising alternative fuels [23-29]. Dual-fuel Spark

Ignition (DFSI) engines have attracted interest from more researchers in recent years [30-37]. DFSI engine can utilise the advantages of ethanol and gasoline by varying their proportion in real-time based on demand. Benefiting from a dual-injection system, in which one fuel can be injected under PFI while the other can be simultaneously injected under Direct Injection (DI). Ethanol with high oxygenated content and high octane number can reduce particle emissions and enhance anti-knock ability. Meanwhile, gasoline can provide higher heating value and volatility, which helps the engine achieve a faster dynamic response. Hence, it is essential to investigate the implementation of OFC in an ethanol-gasoline DFSI engine.

In the ongoing research project named RIVER funded by the Interreg North-West Europe, OFC technology is a primary selection to achieve zero-carbon emissions for Inland Waterway (IW) vessels. Nowadays, most IW vessels rely on IC engines with conventional fuels as the primary power source. However, the dominance of the IC engines would face challenges due to the stricter emission regulations for non-road mobile machinery and worldwide impact on GHG emissions [38][39].

In this paper, a numerical investigation about the implementation of OFC on a practical ethanol-gasoline DFSI engine was conducted. The simulation aims to achieve an equivalent power output of OFC mode with CAC mode, simultaneously reducing the fuel consumption as far as possible. This paper will contribute to an initial understanding of the performance and optimisation methods of ethanol-gasoline DFSI engines under OFC mode, as well as providing a theoretical foundation for the OFC technology implementation in DFSI engines.

2. Numerical method

2.1. Engine specifications and testbed

The numerical study is conducted based on an advanced dual-injection DFSI engine, which specifications are shown in Table 2. The engine has four cylinders, a displacement of 2.0 litres and a

103 compression ratio of 9.6. The fuels used in this study are ethanol and commercial gasoline, as shown
104 in Table 3.

105 **Table 2.** Engine specifications

Items	Content
Engine type	4-cylinder, 4-stroke
Bore × Stroke (mm)	82.5 × 92
Displacement (L)	2.0
Injection type	Dual-injection
Intake type	Turbocharged
Compression ratio	9.6:1
Rated speed (rpm)	5500
Rated power (kW)	160
Maximum Torque (N·m)	320

106

107 **Table 3.** Fuel properties

Fuel type	Ethanol	Gasoline
Chemical formula	C_2H_5OH	C5-C12
Relative molecular mass	46	95-120
Gravimetric oxygen content (%)	34.78	< 1
Research octane number	107	95
Density (20 ℃) (kg/L)	0.789	0.73
Dynamic viscosity (20 ℃) (mPa·s)	1.2	0.52
Kinematic viscosity (20 ℃) (mm^2/s)	1.52	0.71
Surface tension (20 ℃) (N/m)	21.97	22
Boiling range (℃)	78	30-200
Low heating value (kJ/kg)	26900	44300
Latent heat of vaporisation (kJ/kg)	840	370
Laminar flame speed (20 ℃) (m/s)	0.5	0.33
Stoichiometric air-fuel ratio	8.95	14.7

108 The required data for model validation was obtained from the testbed's experimental results given
109 in Fig. 2. During the experiment, the engine's speed, torque and power were controlled and measured
110 by an alternating current dynamometer, a programmable electronic control unit and software INCA.
111 The spark timing was optimised to be the minimum advance for Maximum Brake Torque (MBT) or
112 Knock Limited Spark Advance (KLSA). In order to obtain required combustion characteristics, spark-

plug type pressure sensors (AVL-GH13Z), a charge amplifier (Kistler 5018A) and a combustion analyser (AVL 641) were utilised to measure and analyse the transient in-cylinder pressure signals. The cylinder pressure data were averaged by 200 consecutive cycles to minimise the deviations by cycle-to-cycle variations.

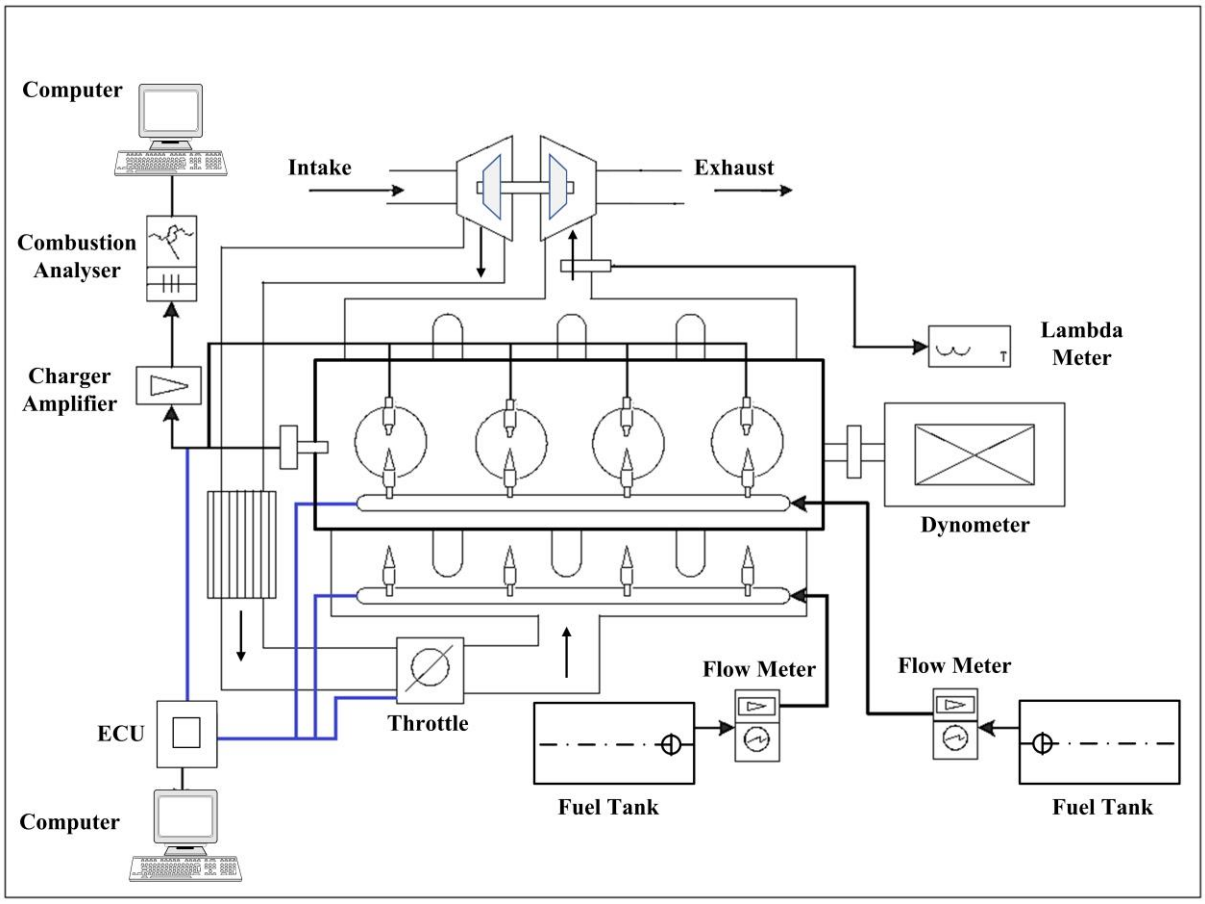

Fig. 2. Schematic view of the testbed

2.2. Model description

To explore the implementation of OFC technology in the DFSI engine, a one-dimensional numerical model was established using software GT-Power, which is an industry-standard simulation tool to predict and analyse engine combustion performance. Furthermore, this software is widely used in academic research for combustion characteristics of SI engines [40][41][42][43]. Some of the fundamental formulas in this model about heat transfer submodel and combustion submodel are

illustrated as follows.

2.2.1. Heat transfer submodel

The heat transfer submodel is set to be 'Woschni model'. It was put forward as a classical method to calculate the instantaneous heat transfer coefficient for IC engines by Woschni in 1967 [44]. The total heat transferred Q_W and heat transfer coefficient h can be summarised as Equation (2) and Equation (3), respectively.

$$Q_W = \int_0^{cycle} \sum_i h\, A_i (T - T_{wi}) d\varphi \tag{2}$$

$$h = 110 d^{-0.2} P^{0.8} T^{-0.53} [C_1 c_m + C_2 \frac{V_S T_1}{P_1 V_1} (P - P_0)]^{0.8} \tag{3}$$

Here, Q_W is total heat transferred; h is heat transfer coefficient; A_i is heat absorbing areas of the surfaces; T_{wi} is mean surface temperature of A_i; T is in-cylinder mean gas temperature; φ is Crank Angle (CA) interval; d is diameter of the cylinder bore; P is cylinder pressure; C_1 is a constant related to airflow velocity coefficient; C_2 is a constant related to combustion chamber; c_m is mean piston speed; V_S is cylinder volume; T_1, P_1 and V_1 are cylinder temperature, pressure and volume at the beginning of compression, respectively. P_0 is cylinder pressure when the engine is started.

2.2.2. Combustion submodel

The 'SI turbulent flame combustion model' is set for combustion submodel in this simulation. This model is qualified for predicting the in-cylinder burn rate, emissions and knocking occurrence from SI engines fuelled with oxygenated fuel [40]. Flame-wall interactions, laminar flame speed, knock and other important aspects are all contained in this model.

The flame-wall interactions can be calculated accurately based on the geometry of combustion chamber, affected by the detailed setting of piston cup, head region and spark location. Fuel dependence should be notably set up in detail based on some customised options, affecting the laminar

flame speed, knock prediction, burned zone kinetics, etc. Laminar flame speed is calculated as the Equations (4), (5) and (6) [45].

$$S_{L,0} = B_m - B_\delta(\delta - \delta_m)^2 \quad (4)$$

$$S_L = S_{L,0}(\frac{T_u}{T_{ref}})^\alpha(\frac{p}{p_{ref}})^\beta = [B_m - B_\delta(\delta - \delta_m)^2]\left(\frac{T_u}{T_{ref}}\right)^\alpha\left(\frac{p}{p_{ref}}\right)^\beta f(D) \quad (5)$$

$$f(D) = 1.0 - 0.75\lambda_{DEM}[1.0 - (1.0 - 0.75\lambda_{DEM}D)^7] \quad (6)$$

Here, $S_{L,0}$ is laminar flame speed at the condition of 298 K and 101.325 kPa; B_m is maximum laminar speed; B_δ is laminar speed roll-off value; δ is in-cylinder equivalence ratio; δ_m is equivalence ratio at maximum speed; S_L is laminar flame speed; T_u is unburned gas temperature; T_{ref} is 298 K; p is pressure; p_{ref} is 101.325 kPa; α is temperature exponent; β is pressure exponent; $f(D)$ is dilution effect; D is mass fraction of the residuals in the unburned zone; λ_{DEM} is dilution effect multiplier.

Besides, the temperature exponent (α) and pressure exponent (β) in Equations (7) and (8) are used for gasoline, while the Equations (9) and (10) are used for ethanol [46][47]. Here, δ is in-cylinder equivalence ratio.

For gasoline:

$$\alpha = 2.4 - 0.271\delta^{3.51} \quad (7)$$

$$\beta = -0.357 + 0.14\delta^{2.77} \quad (8)$$

For ethanol:

$$\alpha = 2.18 - 0.8(\delta - 1) \quad (9)$$

$$\beta = -0.16 + 0.22(\delta - 1) \quad (10)$$

2.3 Key parameters and research approach

In order to better understand the performance characteristics in this study, some parameters are introduced as follows.

Ignition delay (θ_F) is introduced to represent the CA interval between spark timing and φ_{CA10} (where 10% fuel is burned). Combustion duration (θ_C) is introduced to represent the CA interval between φ_{CA10} and φ_{CA90} (where 90% fuel is burned). φ_{CA50} denotes the CA where 50% fuel is burned. φ_{Pmax} denotes the CA location of peak cylinder pressure. The lambda$_{O2}$ is introduced as Equation (11). In Equations (12) and (13), Brake Specific Oxygen Consumption (BSOC) and Brake Specific Fuel Consumption (BSFC) are introduced to analyse oxygen consumption and fuel economy, respectively.

$$lambda_{O2} = \frac{\tau_O}{\tau_{ost}} \tag{11}$$

$$\mathrm{BSOC} = \frac{\tau_O \times 1000}{P} \tag{12}$$

$$\mathrm{BSFC} = \frac{\tau_F \times 1000}{P} \tag{13}$$

Here, τ_O (kg/h) and τ_F (kg/h) denotes the consumption rate of oxygen and gasoline under actual condition, respectively. τ_{ost} (kg/h) represents the oxygen mass flow rate at the stoichiometric condition. P (kW) denotes the engine brake power.

In this research, '2000 rpm-2 bar Brake Mean Effective Pressure (BMEP)' and '2000 rpm-10 bar BMEP' are selected to represent the low load and mid-high (m-h) load of typical engine operating conditions, respectively. In order to simplify the research process and make research purpose clear, the mass ratio of ethanol and gasoline is set to be 1:1. 'E-G' injection strategy represents 50% ethanol PFI and 50% gasoline DI in mass. 'G-E' strategy represents 50% gasoline PFI and 50% ethanol DI. Some key experimental operating parameters and results under CAC mode are shown in Table 4.

Table 4. Experimental operating parameters and results under CAC mode

Items	Content	
Speed (rpm)	2000	2000
BMEP (bar)	2	10
Load	low load	mid-high load
Ambient pressure (bar)	1	1
Ambient temperature (℃)	25	25

Injected fuel temperature (℃)	25	25
DI injection timing (°CA)	420	415
PFI injection timing (°CA)	320	320
Spark timing under E-G	-30.5 °CA (MBT)	-22.2 °CA (KLSA)
Spark timing under G-E	-29.9 °CA (MBT)	-23 °CA (KLSA)
BSFC under E-G (g/kWh)	492.97	294.41
BSFC under G-E (g/kWh)	493.26	294.46
Lambda	1	1

In order to clearly illustrate the research approach of this study, a flow chart is depicted as Fig. 3. First, model validation should be performed based on experimental results at low and mid-high loads to ensure the simulation's accuracy.

Second, CO_2 is used to replace with nitrogen, meantime the throttle opening, oxygen mass fraction, stoichiometric air-fuel ratio and fuel injection timing are all kept constant. The performance characteristics under OFC mode without optimisation are calculated, as well as compared to those of CAC mode.

Third, the engine performance will be optimised by changing intake charge components. Under OFC mode, 2 bar and 10 bar are the BMEP target for low load and mid-high load, respectively. Moreover, BSFC should also be optimised as far as possible.

Finally, the engine performance will be further optimised by utilising Water Injection (WI) strategy. Water is injected directly into the combustion chamber for each cylinder by a separated injector. This strategy has been widely applied to optimise OFC process in ICRC engines [17-22]. The water/fuel mass ratio (R_{wf}) is introduced to parameterise the WI mass in this study, as Equation (14).

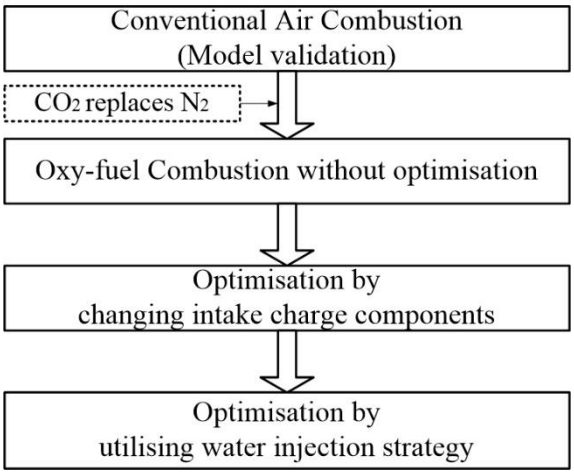

Fig. 3. Flow chart of research approach

$$R_{wf} = \frac{\tau_w}{\tau_f} \tag{14}$$

Here, τ_w (mg/cycle) and τ_f (mg/cycle) denotes the injection quantity of water and fuel per engine cycle, respectively.

3. Results and discussion

3.1 Model validation

This model has been validated with experimental results of the operating condition under CAC mode in Table 4, and the result is shown in Figure 4. It can be seen that the cylinder pressure between experimental and simulation results are obviously in good agreement. The positions and heights of curves' peaks in the simulation are well predicted under E-G and G-E strategies at two different loads, which shows that the model validation can be trusted and acceptable.

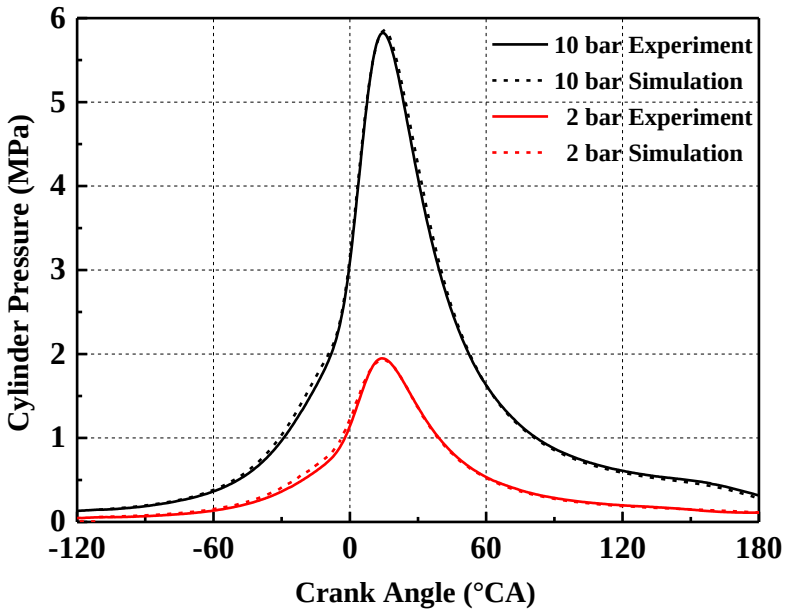

(a) E-G

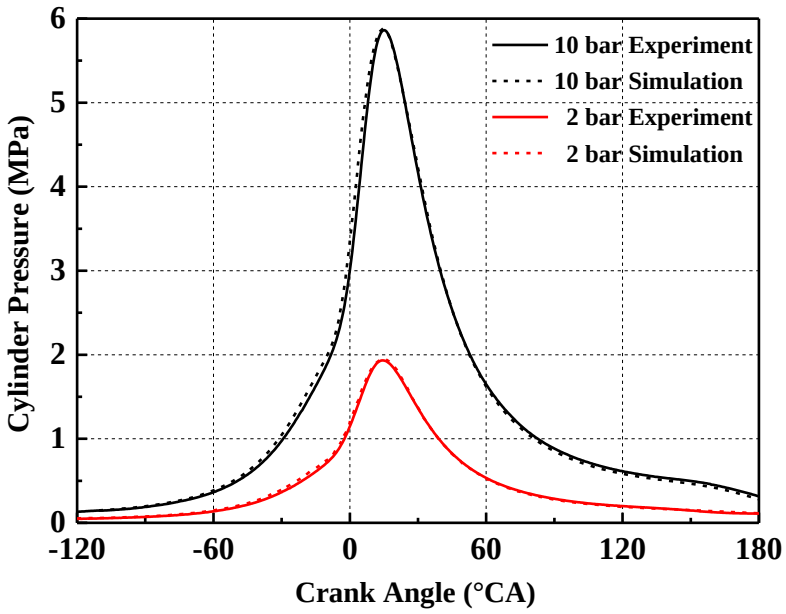

(b) G-E

Fig. 4. Comparison of cylinder pressure between experimental and simulation results at low and mid-high loads

3.2 Performance characteristics under OFC mode without optimisation

In this section, as CO_2 replaces nitrogen, the engine operation is converted into OFC mode. The air-fuel ratio is kept constant at the stoichiometric condition. The throttle opening, oxygen mass fraction, and fuel injection timing remain consistent with CAC mode. Besides, optimal spark timings should be found for improving engine combustion performance under OFC mode.

Fig. 5 illustrates the variation of BMEP and BSFC with varying spark timings under OFC mode. There is a clear deterioration on both BMEP and BSFC under OFC mode at low load compared to CAC mode. The best BMEP is 1.444 bar with the spark timing of -76 °CA under E-G, and 1.516 bar with spark timing of -72 °CA under G-E. Both of them have a significant decline compared with 2 bar of CAC mode. Meanwhile, the corresponding BSFC is 779.728 g/kWh and 778.301 g/kWh, respectively.

At mid-high load, BMEP of OFC mode can achieve 10 bar, which is the same with CAC mode. This is mainly because the avoidance of knocking combustion is easy to be achieved due to the lower thermal diffusivity of CO_2 under OFC mode, so the combustion phase can potentially be advanced for maintaining BMEP. The lowest BSFC is 363.157 g/kWh of E-G and 363.464 g/kWh of G-E at the -64 °CA identified as MBT timing. It indicates that the MBT timing can improve fuel economy under OFC mode, but BSFC is still much higher than 294.41g/kWh and 294.46 g/kWh of CAC mode.

These characteristics can be explained by the net Heat Release Rate (HRR) curves, as shown in Fig. 6 and Fig. 7. The HRR curves of CAC mode from experimental results are also plotted for comparisons. It shows that the peaks decrease from around 33 J/CA of CAC mode to 20 J/CA of OFC mode at low load, and a decline from 110 J/CA to 80 J/CA at mid-high load. These findings can be attributed to the difference in CO_2 and nitrogen properties in Table 1. The thermal diffusivity and oxygen diffusivity in CO_2 are much lower than those of nitrogen. Hence, the rate of flame propagation and heat transfer during combustion process will be reduced, resulting in more heat loss than CAC mode. Although the thermal conductivity of CO_2 is a bit higher than nitrogen, the offset effects are relatively weak.

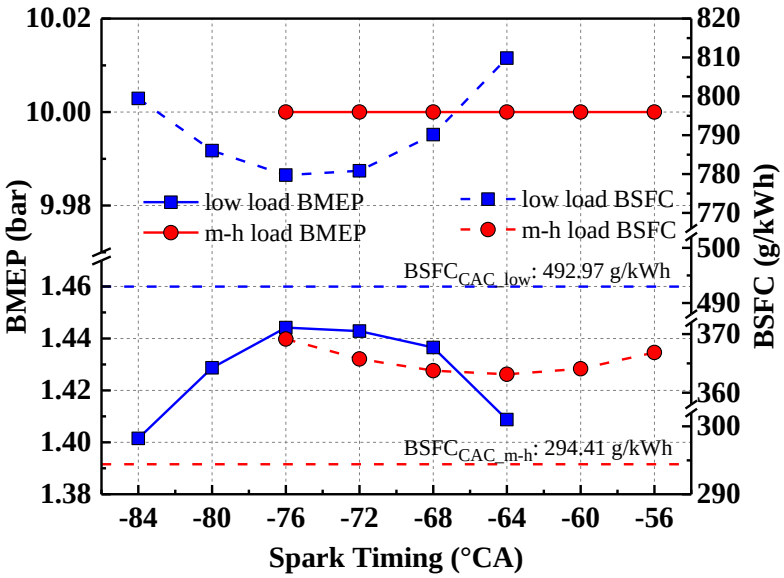

(a) E-G

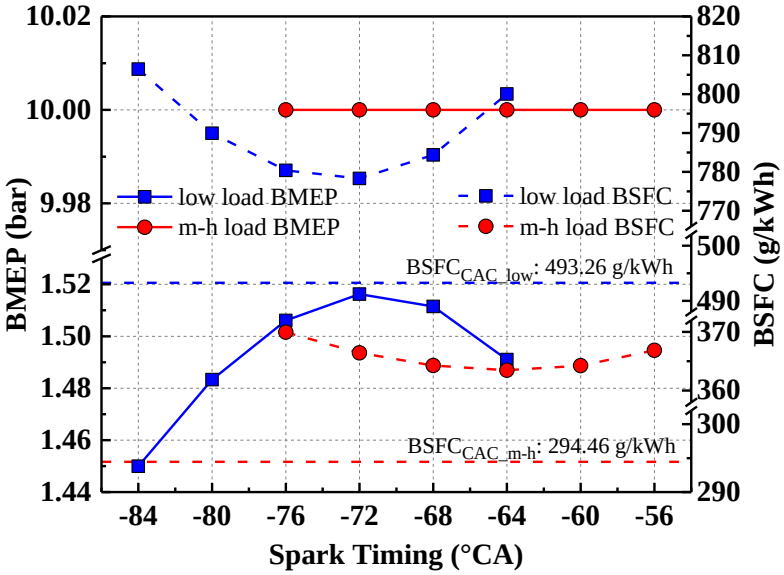

(b) G-E

Fig. 5. BMEP and BSFC with varying spark timings under OFC mode

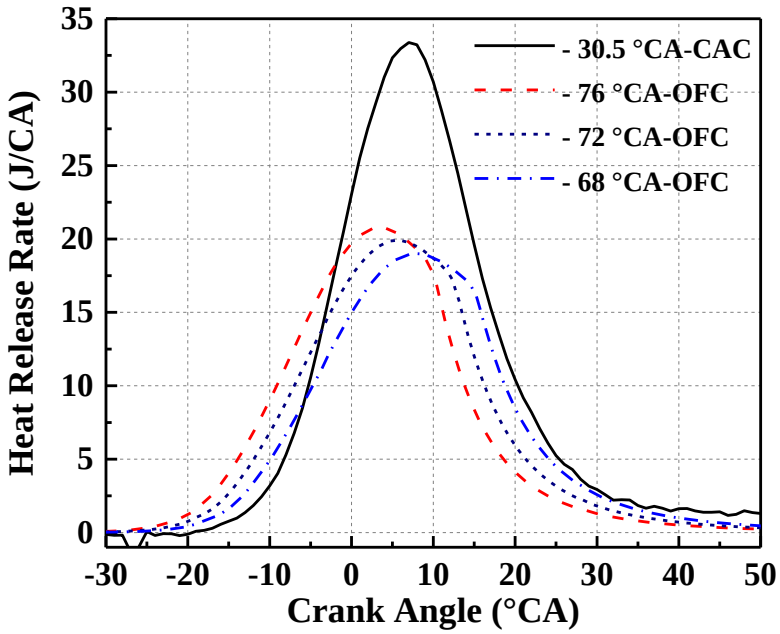

(a) E-G

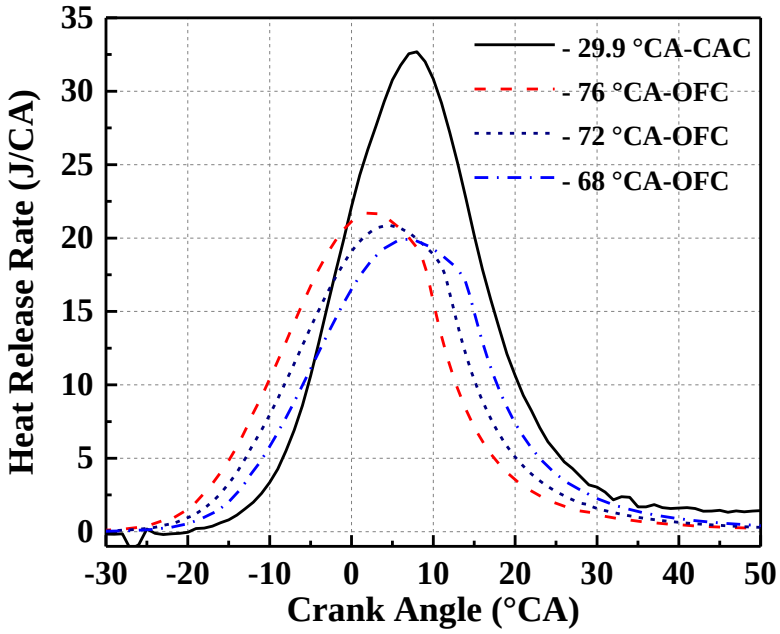

(b) G-E

Fig. 6. HRR with varying spark timings at low load

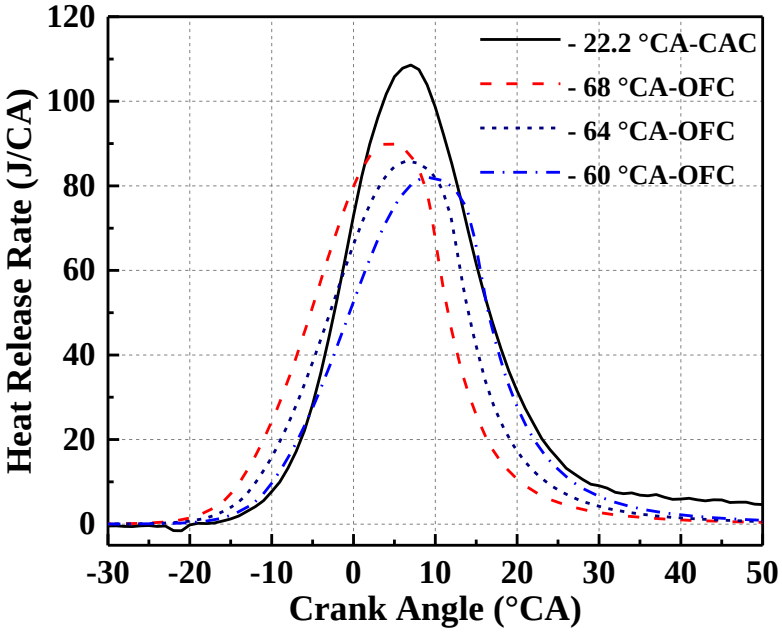

(a) E-G

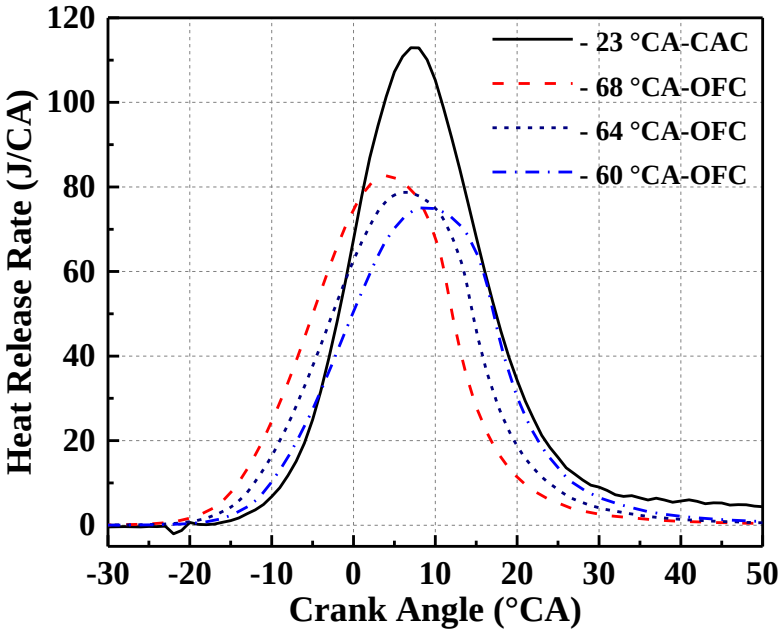

(b) G-E

Fig. 7. HRR with varying spark timings at mid-high load

3.3 Performance optimisation by changing intake charge components

In order to facilitate the implementation of OFC technology in DFSI engines, the performance optimisation on BMEP and BSFC should be highly valued. Oxygen is essential to the combustion process, so it is possible to optimise combustion performance by changing intake charge components.

Furthermore, as higher oxygen fraction will increase the cost, the maximum oxygen mass fraction is limited to 29% in this research, which is set to 21%, 23.3%, 25%, 27% and 29%. The corresponding $lambda_{O2}$ is each 0.901, 1, 1.073, 1.159 and 1.245. When the oxygen fraction changes, the throttle position remains unchanged opening percentage. MBT or KLSA spark timing is also applied to all conditions in this section for maximising BMEP or thermal efficiency.

Fig. 8 and Fig. 9 shows the effects of intake charge components on mean in-cylinder temperature at low load and mid-high load, respectively. In Fig. 8, a good agreement can be observed to the curves' changing trend under E-G and G-E. As the oxygen fraction increases, there is a short delay and a slight rise in the curve's peak, which increases from 2044.16 K to 2055.25 K under E-G, and 2056.11 K to 2073.3 K under G-E. At mid-high load, Fig. 9 illustrates the curves' peaks remain stable around 2110 K and 2090 K under E-G and G-E, respectively.

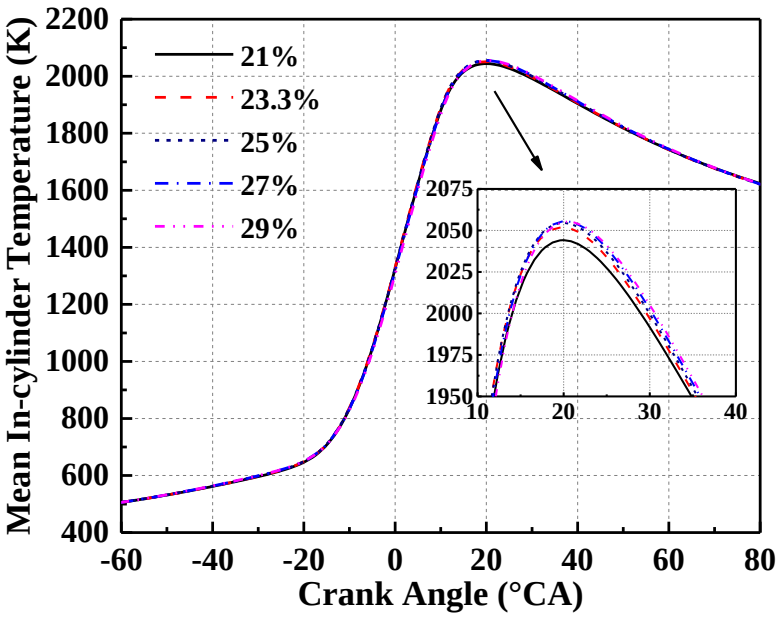

(a) E-G

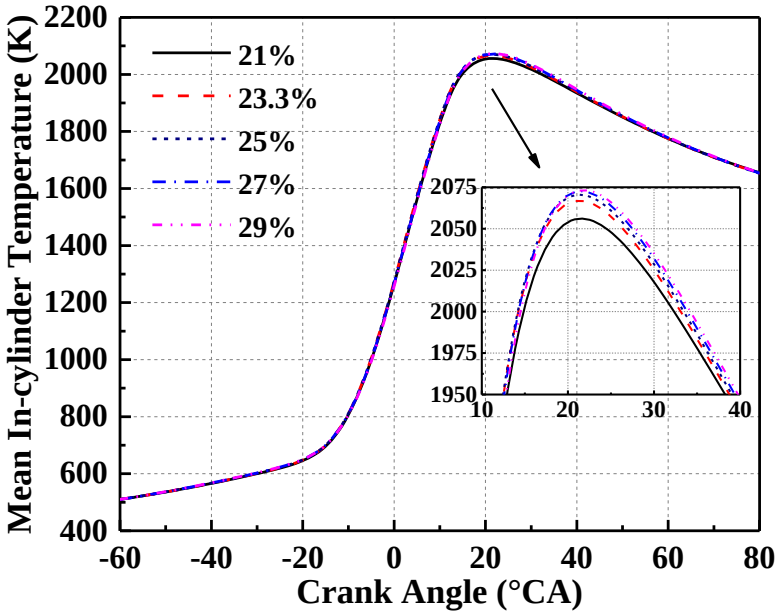

(b) G-E

Fig. 8. Effects of intake charge components on in-cylinder temperature at low load

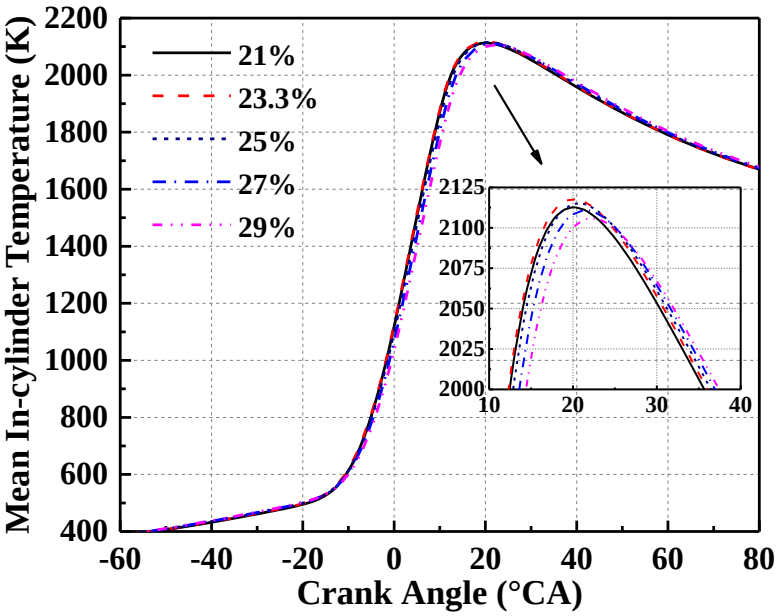

(a) E-G

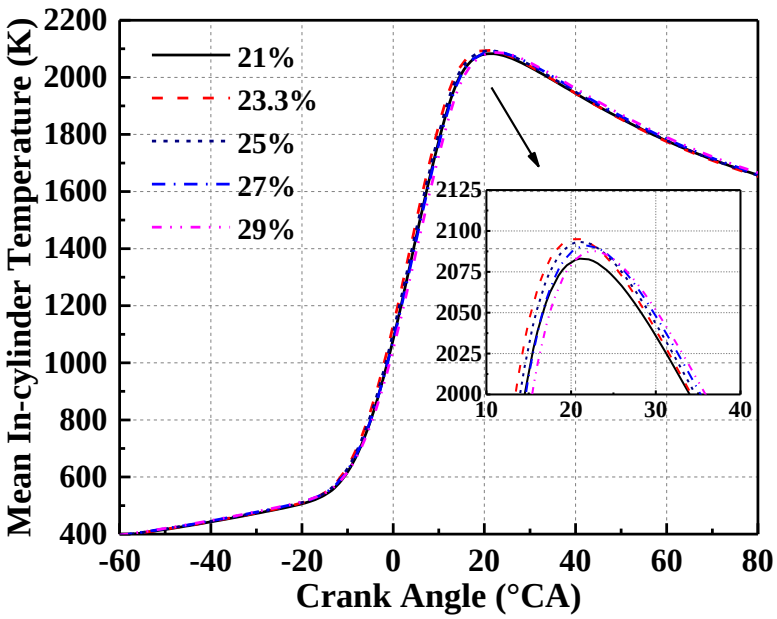

(b) G-E

Fig. 9. Effects of intake charge components on in-cylinder temperature at mid-high load

Fig. 10 and Fig. 11 depicts the effects of intake charge components on variations of θ_F and θ_C, respectively.

The θ_F has an evident growth with the increase of oxygen fraction at mid-high load. It increases quickly by 0.92 degrees and 1.38 degrees under E-G and G-E respectively, as oxygen fraction increases from 21% to 23.3%. Followed by a further growth of approximately 1.2 degrees when oxygen fraction rises to 29%. It is because the rich fuel-oxygen mixture ($lambda_{O2}$ = 0.901) under the condition of 21% oxygen fraction can help accelerate the laminar burning velocity, reducing the flame development period [45][48][49]. However, the acceleration of burning velocity is partially offset by the negative effects of increased CO_2 fraction. Furthermore, the offset effects are enhanced at low load, which θ_F under 21% oxygen fraction condition only reduces approximately 0.4 degrees than that of 29% oxygen fraction condition. Besides, the θ_F of G-E is lower than that of E-G, mainly due to the ethanol's high oxygen content and high laminar flame speed, as presented in Table 3. The difference becomes noticeable at low load. Because compared with mid-high load, ethanol injection

quantity per operating cycle is much lower at low load, mitigating the suppression on the flame propagation velocity in the initial stage by the cooling effect of direct-injected ethanol.

Regarding the θ_C, a good agreement is observed for the four curves' trend with the variations of oxygen fraction in Fig. 11. With oxygen fraction increases from 21% to 29%, θ_C continues upward approximately 0.8 degrees and 1.5 degrees at low load and mid-high load, respectively. This suggests that a slight lean fuel-oxygen mixture ($lambda_{O2}$ = 1.073, 1.159 and 1.245) brings adverse effects on the flame burning rate, which simultaneously overcome the positive effects from reduced CO_2 fraction.

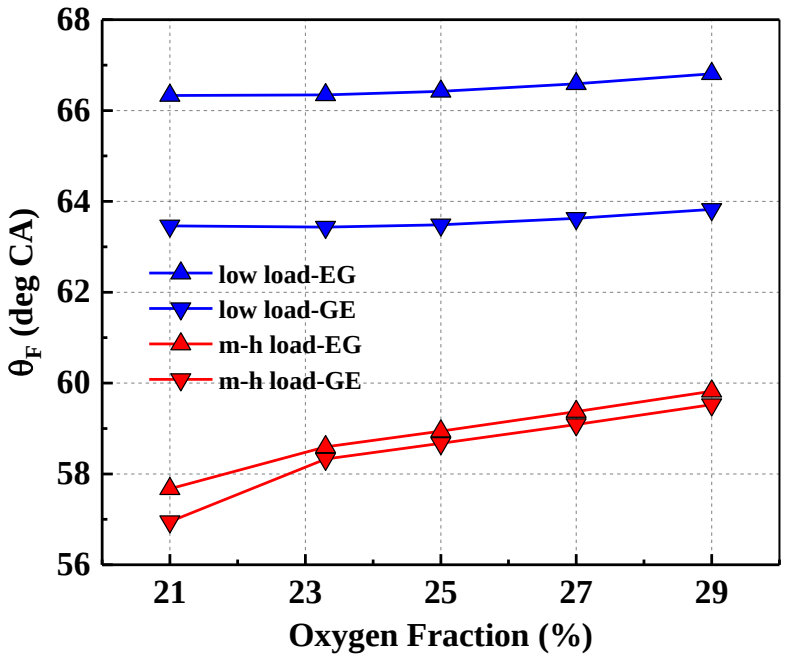

Fig. 10. Effects of intake charge components on θ_F

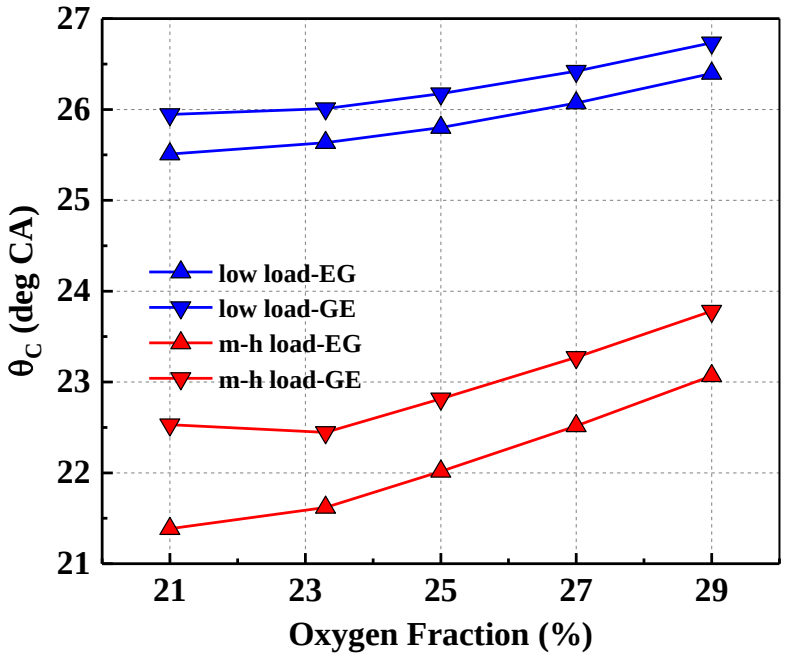

320

321 **Fig. 11.** Effects of intake charge components on θ_C

322

323 Fig. 12 and Fig. 13 shows the effects of intake charge components on performance characteristics
324 at low and mid-high loads, including BMEP, BSFC and BSOC.

325 At low load, with oxygen fraction increases from 21% to 29%, BMEP increase approximately
326 0.04 bar, which is 1.473 bar of E-G and 1.547 bar of G-E. Meantime, BSFC has a decline of 32 g/kWh,
327 but BSOC has a 32.5% growth approximately. As BMEP is kept at 10 bar for each condition at mid-
328 high load, it is only necessary to show BSFC and BSOC in Fig. 13. With the oxygen fraction varies
329 from 21% to 29%, BSFC reduces about 2.4% while the BSOC has a rise of 34.8 %. This is because
330 the specific heat ratio is enhanced over the expansion stroke with the increased oxygen fraction,
331 leading to higher conversion efficiency and stronger work for per unit mass of fuel.

332

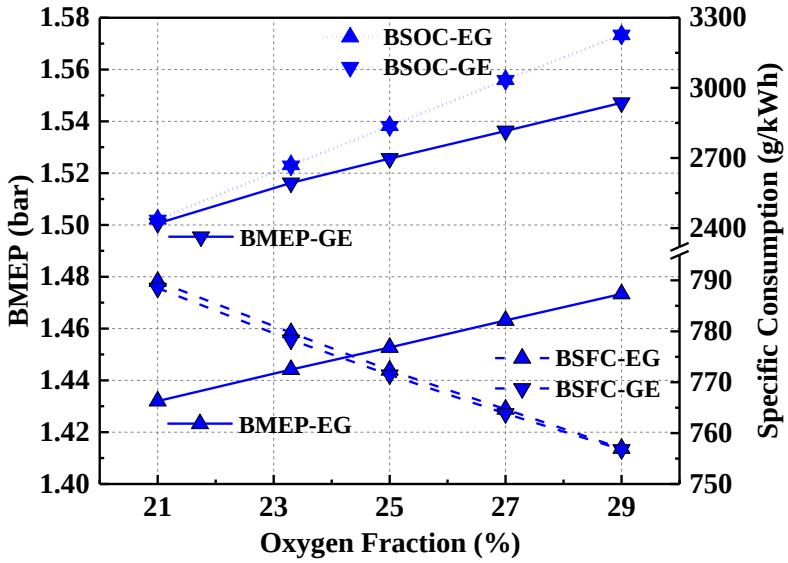

Fig. 12. Effects of intake charge components on BMEP, BSFC and BSOC at low load

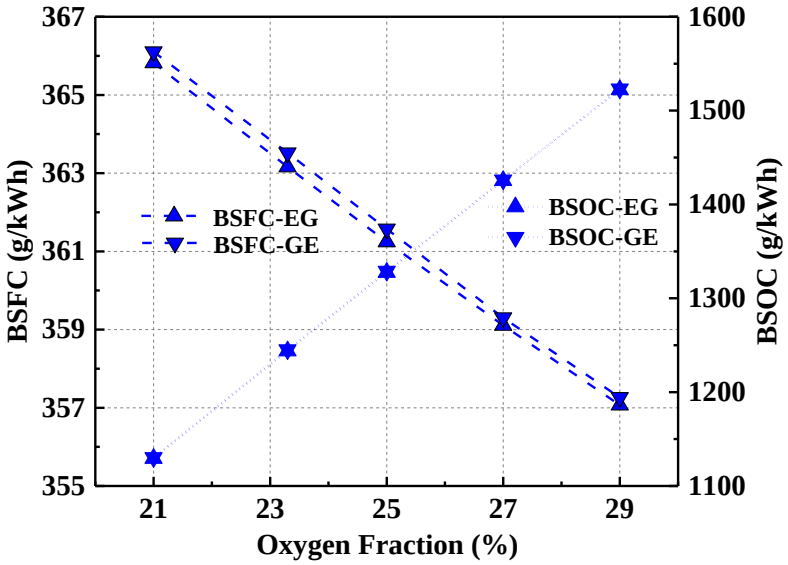

Fig. 13. Effects of intake charge components on BSFC and BSOC at mid-high load

3.4 Performance optimisation by utilizing Water Injection (WI) strategy

Fig. 14 and Fig.15 shows the effects of WI strategy on BMEP and BSFC at low load under 29% oxygen fraction.

Regarding the effects of R_{wf} for a fixed WI timing, it is observed that BMEP slightly increases at first then decreases as R_{wf} ascends. This trend becomes more evident under an early WI timing. Such as under -80 °CA WI timing, BMEP increases from 1.487 bar at R_{wf} = 0.1 to 1.492 bar at R_{wf} = 0.2, followed by a sharp decline to 1.458 bar at R_{wf} = 0.5 under E-G; G-E's BMEP finally slides

to a 1.505 bar. As R_{wf} rises to 0.5, BSFC deteriorates to 781.17 g/kWh and 804.25 g/kWh under E-G and G-E, respectively.

Regarding the effects of WI timing, it is negligible by adding a small quantity of water, but it becomes obvious by injecting more water. For example, at R_{wf} = 0.5, BMEP and BSFC have a sharp deterioration as WI timing advances to -80 °CA. This can be more clearly explained by the effects of WI timing on φ_{CA50}, φ_{Pmax} and HRR in Fig. 16. With the advance of WI timing from -40 °CA to -60 °CA, φ_{CA50} and φ_{Pmax} are respectively retarded to 8 °CA and 14.59 °CA, which are still within the appropriate range for high engine efficiency. Further advancing WI timing results in the postponement of combustion phasing by stronger cooling effects from the heat absorption of injected water.

By utilising WI strategy at low load, BMEP of E-G and G-E each can be improved to 1.495 bar and 1.561 bar, which has 0.051 bar and 0.045 bar increase compared to maximum BMEP under unoptimised conditions in Fig. 5, respectively. This suggests that appropriate WI mass and timing has a small positive impact on BMEP. Because the evaporation process of injected water can reduce cylinder pressure and temperature, leading to a reduction in energy loss during the compression stroke. Simulation results also show that the lowest BSFC under E-G and G-E each can be further reduced to 750.997 g/kWh and 754.803 g/kWh, which is about 3.35% less than that of unoptimised conditions.

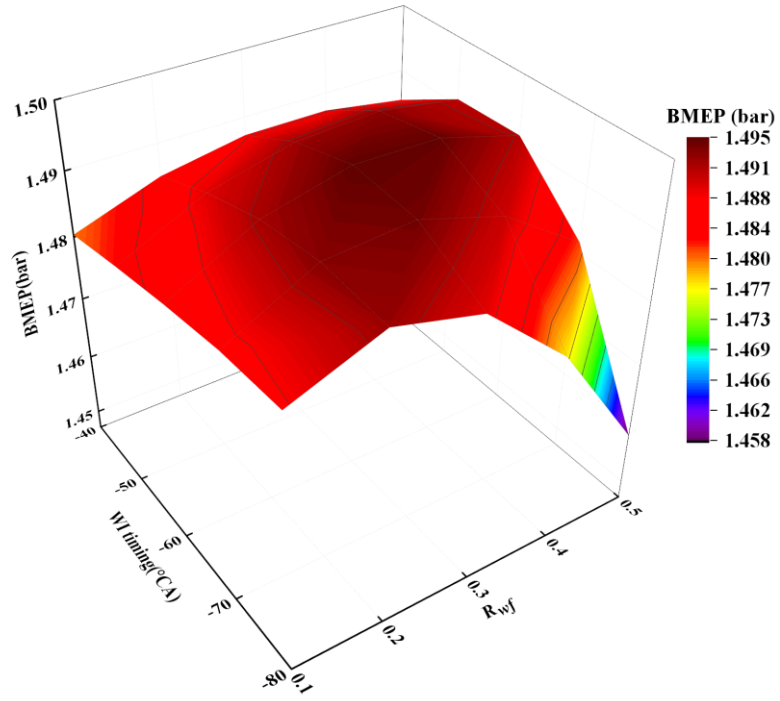

(a) E-G

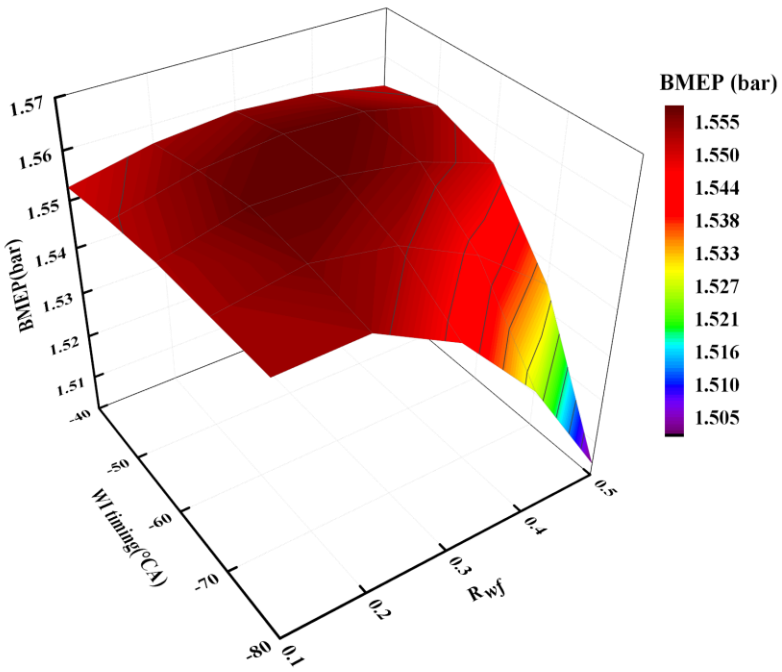

(b) G-E

Fig. 14. Effects of WI strategy on BMEP at low load

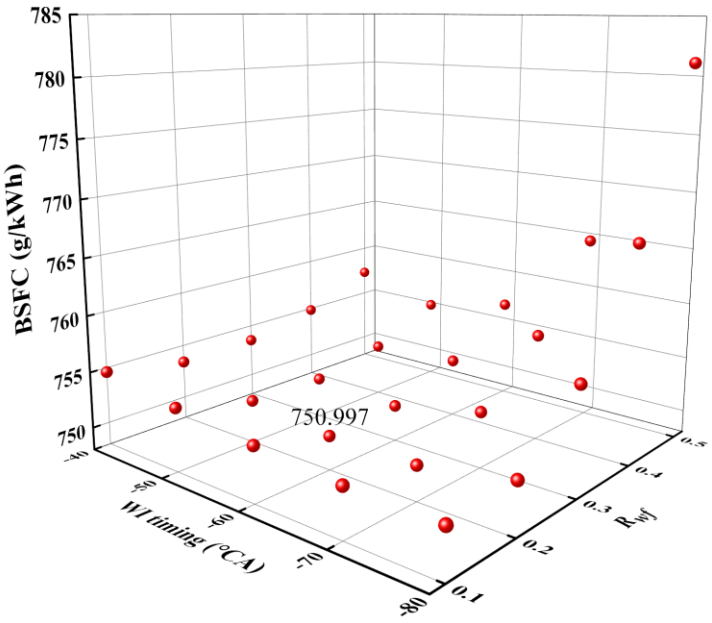

(a) E-G

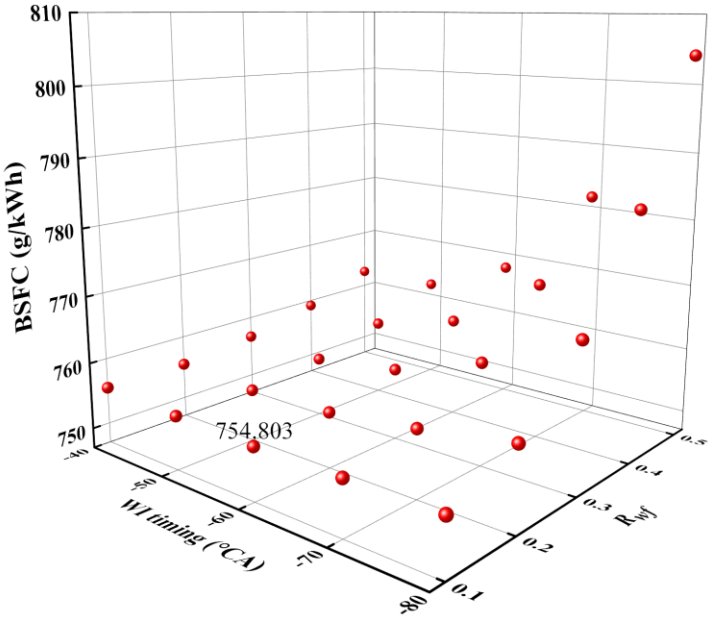

(b) G-E

Fig. 15. Effects of WI strategy on BSFC at low load

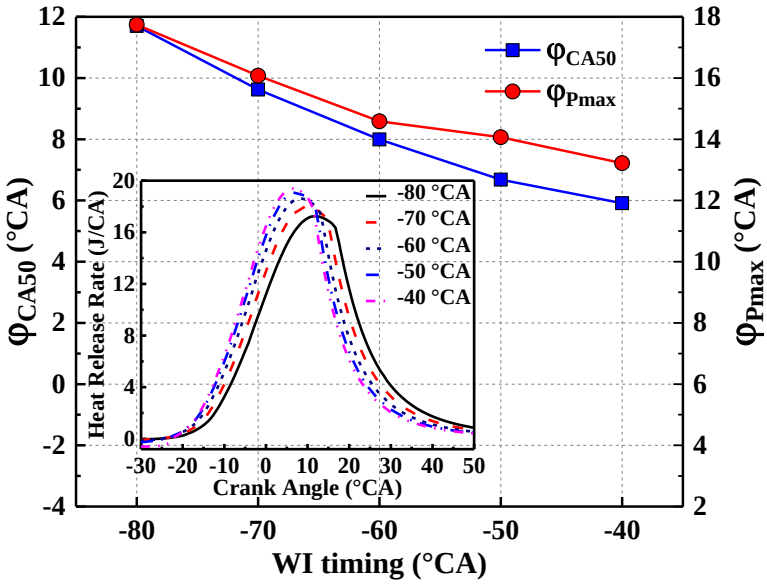

372

373 **Fig. 16.** Effects of WI timing on φ_{CA50}, φ_{Pmax} and HRR (R_{wf} = 0.5, E-G, low load)

374

375 Fig. 17 shows the effects of WI strategy on BSFC at mid-high load under 29% oxygen fraction.
376 It can be seen that the lowest BSFC occurs at the condition of R_{wf} = 0.1, which is 356.72 g/kWh
377 and 356.668 g/kWh under E-G and G-E, respectively. Compared to the unoptimised conditions in Fig.
378 5, BSFC has a reduction of 1.82% at mid-high load.

379 It is also observed that BSFC is less affected by WI timing but is sensitive to R_{wf} at mid-high
380 load. As R_{wf} increases from 0.1 to 0.5, a deterioration for BSFC is between 2.062 g/kWh to 4.463
381 g/kWh. Fig. 18 shows that by R_{wf} increasing from 0.1 to 0.5, φ_{CA50} retards to 11.48 °CA and the
382 HRR's peak is postponed by 4.33 °CA. In the meantime, φ_{Pmax} is retarded from 15.74 °CA to
383 17.99 °CA. It indicates that enhanced cooling effect from excessive amount of water prior to spark
384 timing could slow down the combustion process and reduce the peak cylinder pressure, which leads
385 to a drop in engine efficiency.

386

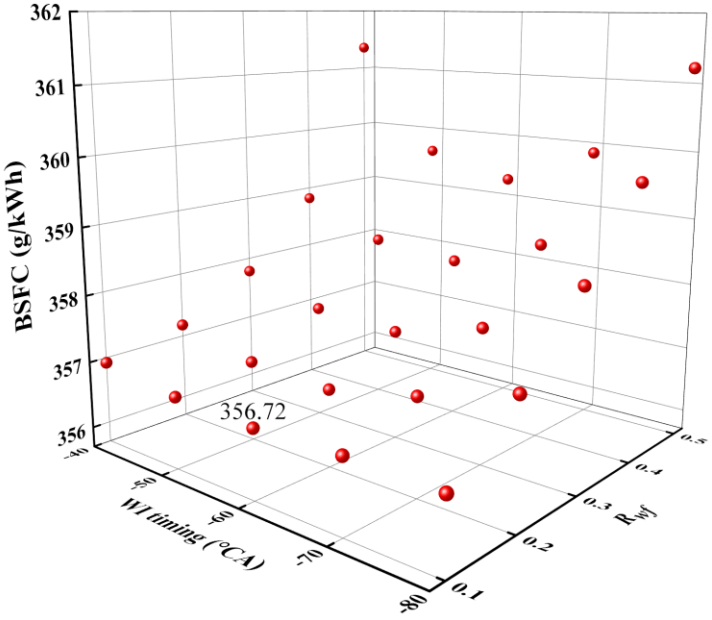

(a) E-G

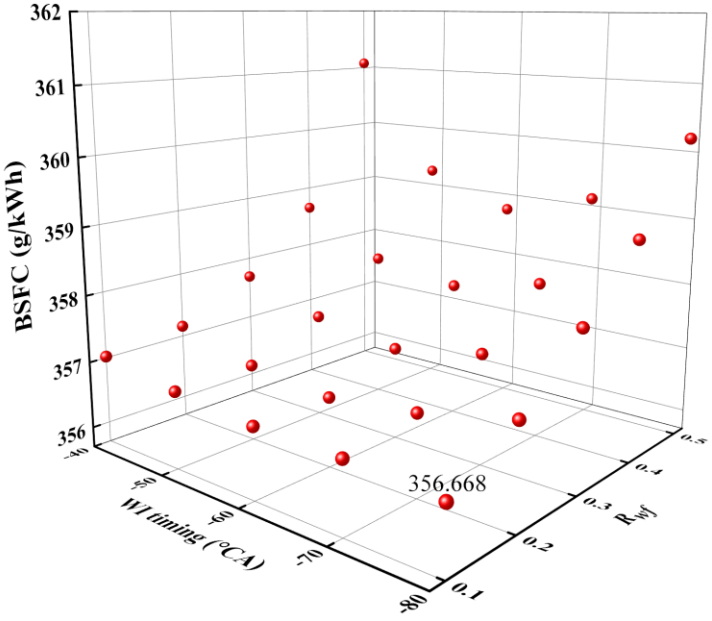

(b) G-E

Fig. 17. Effects of WI strategy on BSFC at mid-high load

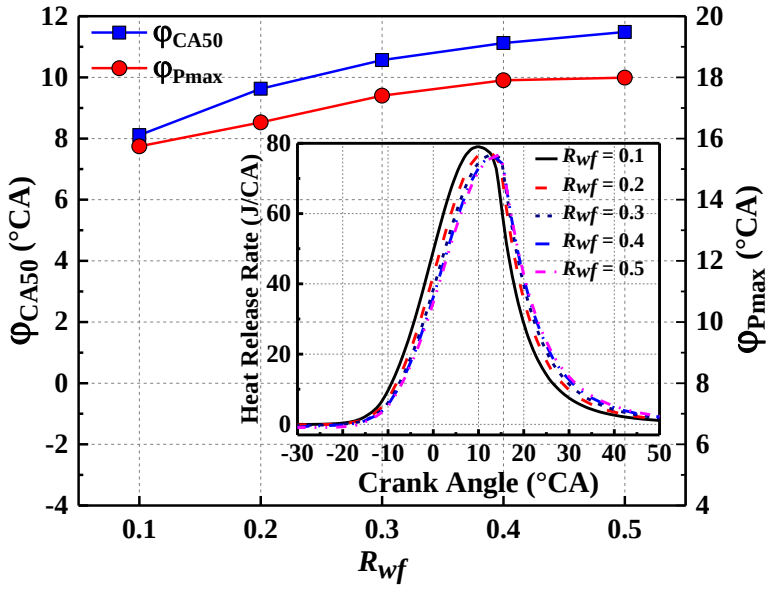

Fig. 18. Effects of WI mass on φ_{CA50}, φ_{Pmax} and HRR (WI timing = -80 °CA, E-G, mid-high load)

4. Conclusion

A numerical investigation on implementing OFC technology on an ethanol-gasoline DFSI engine was conducted at low and mid-high loads. The engine performance was optimised by changing intake charge components and utilising WI strategy. The main conclusions of this study can be summarised as follows:

(1) Under OFC mode with other optimisation at low load, BMEP is 1.444 bar for E-G and 1.516 bar under G-E, which has a decline compared to 2 bar BMEP of CAC mode. At mid-high load, BMEP can achieve the same value with CAC mode. However, the peak of HRR have an evident decrease, and BSFC also has a considerable deterioration.

(2) With oxygen fraction increases from 21% to 29%, the slight lean fuel-oxygen mixture can cause a small extension to θ_F and θ_C. Meantime, there is a clear benefit for BSFC because the specific heat ratio can be enhanced over the expansion stroke with increased oxygen fraction.

(3) The enhanced cooling effect from excessive amount of water or inopportune WI timings could slow down the combustion process, which leads to a deterioration in BSFC.

(4) It is a practical method to optimise DFSI engine performance under OFC mode by improving oxygen fraction and utilising appropriate WI strategies. In this way, BMEP increases approximately 0.05 bar at low load. BSFC has a reduction of 3.35% and 1.82% at low load and mid-high load, respectively.

Based on this study, an understanding of the performance and optimisation of ethanol-gasoline DFSI engines under OFC mode are reached. It is beneficial to provide a theoretical foundation to future works that aim to further improve engine efficiency and cost competitiveness of OFC mode with various optimisation methods, such as different intake charge components, fuel injection strategies, variable valve actuation strategies, etc.

Acknowledgement

This work is financially supported by the Interreg North-West Europe (Project No. NWE553).

Reference

[1] Kanniche M, Gros-Bonnivard R, Jaud P, et al. Pre-combustion, post-combustion and oxy-combustion in thermal power plant for CO_2 capture. Applied Thermal Engineering, 2010, 30(1): 53-62.

[2] Wang M, Joel A S, Ramshaw C, et al. Process intensification for post-combustion CO_2 capture with chemical absorption: A critical review. Applied Energy, 2015, 158: 275-291.

[3] Bandhauer T M, Garimella S, Fuller T F. A critical review of thermal issues in lithium-ion batteries. Journal of the Electrochemical Society, 2011, 158(3): R1.

[4] Lyu Y, Siddique A R M, Majid S H, et al. Electric vehicle battery thermal management system with thermoelectric cooling. Energy Reports, 2019, 5: 822-827.

[5] Zheng G, Peng Z. Life Cycle Assessment (LCA) of BEV's environmental benefits for meeting the challenge of ICExit (Internal Combustion Engine Exit). Energy Reports, 2021, 7: 1203-1216.

[6] Yaverbaum, L. Fluidized Bed Combustion of Coal and Waste Materials; Noyes Data Corp.: Park Ridge, NJ, 1977.

[7] Wall T, Liu Y, Spero C, et al. An overview on oxyfuel coal combustion—State of the art research and technology development. Chemical engineering research and design, 2009, 87(8): 1003-1016.

[8] Chen L, Yong S Z, Ghoniem A F. Oxy-fuel combustion of pulverized coal: Characterization, fundamentals, stabilization and CFD modeling. Progress in energy and combustion science, 2012, 38(2): 156-214.

[9] Thompson R V, Fowler A. Development of a depth independent closed cycle diesel engine. Offshore Technology Conference. Offshore Technology Conference, 1981.
[10] Shaw R, Oman H. Non-air working fluids for closed-cycle diesel engines. Proc., Intersoc. Energy Convers. Eng. Conf.;(United States). The Boeing Company, Seattle, Washington, 1983, 2(CONF-830812-).
[11] Wu H W, Shu C T. Effects of operating parameters on steady and transient behaviors of a closed cycle diesel engine. Energy conversion and management, 2006, 47(15-16): 2070-2080.
[12] Wu H W, Wu Z Y, Yang J Y, et al. Combustion characteristics of a closed cycle diesel engine with different intake gas contents. Applied thermal engineering, 2009, 29(5-6): 848-858.
[13] Wu H W, Wang R H, Chen Y C, et al. Influence of port-inducted ethanol or gasoline on combustion and emission of a closed cycle diesel engine. Energy, 2014, 64: 259-267.
[14] Mobasheri R, Aitouche A, Peng Z, et al. Influence of Oxy-Fuel Combustion on Engine Operating Conditions and Combustion Characteristics in a High Speed Direct Injection (HSDI) Diesel Engine under Homogenous Charge Compression Ignition (HCCI) Mode. SAE Technical Paper, 2020.
[15] Li X, Peng Z, Ajmal T, et al. A feasibility study of implementation of oxy-fuel combustion on a practical diesel engine at the economical oxygen-fuel ratios by computer simulation. Advances in Mechanical Engineering, 2020, 12(12): 1687814020980182.
[16] Bilger R W. Zero release combustion technologies and the oxygen economy. Fifth International Conference on Technologies and Combustion for a Clean Environment, Lisbon, Portugal, Jul. 1999: 12-15.
[17] Bilger R W, Wu Z. Carbon capture for automobiles using internal combustion Rankine cycle engines. Journal of Engineering for Gas Turbines and Power, 2009, 131(3).
[18] Yu X, Wu Z, Fu L, et al. Study of combustion characteristics of a quasi internal combustion rankine cycle engine. SAE Technical Paper, 2013.
[19] Yu X, Wu Z, Wang C, et al. Study of the combustion and emission characteristics of a quasi ICRC engine under different engine loads. SAE Technical Paper, 2014.
[20] Fu L, Wu Z, Li L, et al. Effect of Water Injection Temperature on Characteristics of Combustion and Emissions for Internal Combustion Rankine Cycle Engine. SAE Technical Paper, 2014.
[21] Wu Z J, Yu X, Fu L Z, et al. A high efficiency oxyfuel internal combustion engine cycle with water direct injection for waste heat recovery. Energy, 2014, 70: 110-120.
[22] Wu Z, Yu X, Fu L, et al. Experimental study of the effect of water injection on the cycle performance of an internal-combustion Rankine cycle engine. Proceedings of the Institution of Mechanical Engineers, Part D: Journal of Automobile Engineering, 2014, 228(5): 580-588.
[23] Tartakovsky L, Baibikov V, Veinblat M. Comparative performance analysis of SI engine fed by ethanol and methanol reforming products. SAE Technical Paper, 2013.
[24] Huang H, Liu Q, Wang Q, et al. Experimental investigation of particle emissions under different EGR ratios on a diesel engine fueled by blends of diesel/gasoline/n-butanol. Energy Conversion and Management, 2016, 121: 212-223.
[25] Huang H, Wang Q, Shi C, et al. Comparative study of effects of pilot injection and fuel properties on low temperature combustion in diesel engine under a medium EGR rate. Applied energy, 2016, 179: 1194-1208.
[26] Huang H, Liu Q, Teng W, et al. Improvement of combustion performance and emissions in diesel engines by fueling n-butanol/diesel/PODE3–4 mixtures. Applied Energy, 2018, 227: 38-48.

[27] Li X, Pei Y, Qin J, et al. Effect of ultra-high injection pressure up to 50 MPa on macroscopic spray characteristics of a multi-hole gasoline direct injection injector fueled with ethanol. Proceedings of the Institution of Mechanical Engineers, Part D: Journal of Automobile Engineering, 2018, 232(8): 1092-1104.

[28] Venu H, Raju V D, Subramani L. Combined effect of influence of nano additives, combustion chamber geometry and injection timing in a DI diesel engine fuelled with ternary (diesel-biodiesel-ethanol) blends. Energy, 2019, 174: 386-406.

[29] Chen Z, Wang L, Zeng K. Comparative study of combustion process and cycle-by-cycle variations of spark-ignition engine fueled with pure methanol, ethanol, and n-butanol at various air–fuel ratios. Fuel, 2019, 254: 115683.

[30] Daniel R, Xu H, Wang C, et al. Gaseous and particulate matter emissions of biofuel blends in dual-injection compared to direct-injection and port injection. Applied energy, 2013, 105: 252-261.

[31] Zhuang Y, Hong G. Primary investigation to leveraging effect of using ethanol fuel on reducing gasoline fuel consumption. Fuel, 2013, 105: 425-431.

[32] Zhuang Y, Hong G. The effect of direct injection timing and pressure on engine performance in an ethanol direct injection plus gasoline port injection (EDI+ GPI) SI engine. SAE Technical Paper, 2013.

[33] Zhuang Y, Hong G. Effects of direct injection timing of ethanol fuel on engine knock and lean burn in a port injection gasoline engine. Fuel, 2014, 135: 27-37.

[34] Wang Z, Liu H, Long Y, et al. Comparative study on alcohols–gasoline and gasoline–alcohols dual-fuel spark ignition (DFSI) combustion for high load extension and high fuel efficiency. Energy, 2015, 82: 395-405.

[35] Liu H, Wang Z, Long Y, et al. Dual-Fuel Spark Ignition (DFSI) combustion fuelled with different alcohols and gasoline for fuel efficiency. Fuel, 2015, 157: 255-260.

[36] Liu H, Wang Z, Long Y, et al. Comparative study on alcohol–gasoline and gasoline–alcohol Dual-Fuel Spark Ignition (DFSI) combustion for engine particle number (PN) reduction. Fuel, 2015, 159: 250-258.

[37] Zhuang Y, Zhu G, Gong Z, et al. Experimental and numerical investigation of performance of an ethanol-gasoline dual-injection engine. Energy, 2019, 186: 115835.

[38] Waluś K J, Warguła Ł, Krawiec P, et al. Legal regulations of restrictions of air pollution made by non-road mobile machinery—the case study for Europe: a review. Environmental Science and Pollution Research, 2018, 25(4): 3243-3259.

[39] Lajunen A, Sainio P, Laurila L, et al. Overview of powertrain electrification and future scenarios for non-road mobile machinery. Energies, 2018, 11(5): 1184.

[40] Liu K, Li Y, Yang J, et al. Comprehensive study of key operating parameters on combustion characteristics of butanol-gasoline blends in a high speed SI engine. Applied Energy, 2018, 212: 13-32.

[41] Teodosio L, Pirrello D, Berni F, et al. Impact of intake valve strategies on fuel consumption and knock tendency of a spark ignition engine. Applied Energy, 2018, 216: 91-104.

[42] Tornatore C, Bozza F, De Bellis V, et al. Experimental and numerical study on the influence of cooled EGR on knock tendency, performance and emissions of a downsized spark-ignition engine. Energy, 2019, 172: 968-976.

[43] Tian Z, Zhen X, Wang Y, et al. Combustion and emission characteristics of n-butanol-gasoline blends in SI direct injection gasoline engine. Renewable Energy, 2020, 146: 267-279.

[44] Woschni, G., A universally applicable equation for the instantaneous heat transfer coefficient in the internal combustion engine. No. 670931. SAE Technical paper, 1967.
[45] Heywood, J.B., "Internal Combustion Engine Fundamentals (2nd edit)." McGraw-Hill, 2018.
[46] Rhodes D B, Keck J C. Laminar burning speed measurements of indolene-air-diluent mixtures at high pressures and temperatures. SAE Transactions, 1985: 23-35.
[47] Hara T, Tanoue K. Laminar flame speed of ethanol, n-heptane, iso-octane air mixtures. JSAE paper, 2006, 20068518.
[48] Metghalchi M, Keck J C. Burning velocities of mixtures of air with methanol, isooctane, and indolene at high pressure and temperature. Combustion and flame, 1982, 48: 191-210.
[49] Milton B E, Keck J C. Laminar burning velocities in stoichiometric hydrogen and hydrogen-hydrocarbon gas mixtures. Combustion and Flame, 1984, 58(1): 13-22.